Macromolecules
ARTICLE

Macromolecules **2010**, *43*, 5433–5441 **5433**
DOI: 10.1021/ma100424c

Equilibrium Phases for Thin Films of Polymer Blend Solutions

Mireille Souche* and Nigel Clarke

Department of Chemistry, University of Durham, Durham DH1 3LE, U.K.

Received February 25, 2010; Revised Manuscript Received April 28, 2010

ABSTRACT: We investigate the structure of thin films of polymer blend solutions at equilibrium, taking into account the influence of the solvent concentration. Concentration profiles are obtained by numerical integration of the Hamiltonian flow associated with the mean-field Flory−Huggins−de Gennes theory supplemented by appropriate boundary terms. We focus, in particular, on the case of symmetric polymer blend solutions confined between walls that are antisymmetric with respect to both polymers and symmetric with respect to the solvent. It is shown that, as the system evolves from the one-phase region to the two-phase region, the equilibrium structure of the film undergoes a transition from a monolayer to a bilayer type of structure. Then, depending on whether T is, respectively, greater or smaller than the wetting transition temperature of the solvent free polymer blend, the equilibrium configuration either remains a bilayer or becomes a laterally phase separated structure as solvent is removed from the film. We finally uncover a complete family of new unstable solutions having no analogues in the solvent free case and exhibiting a possibly chaotic behavior of the system.

1. Introduction

The thermodynamics of polymer blend thin films has been largely studied during the past decades. From a theoretical point of view, mean-field calculations have been used extensively to predict their equilibrium configurations. However, to the authors' knowledge, the actual role of solvent in confined polymer blend solutions is still an open question. In this paper we provide the first systematic study of the equilibrium phases of thin films of polymer blend solutions, as an initial step toward a complete analysis of their dynamics. Self-consistent field calculations have proven very efficient in determining qualitative as well as quantitative features of such systems.[1,2] In order to describe the concentration profiles inside the films, another approach, initially developed to describe wetting in semi-infinite systems,[3,4] consists of minimizing the Flory−Huggins−de Gennes free energy supplemented by interfacial terms of order two in local concentrations.[5,6] The authors recently proposed a Hamiltonian reformulation of this mean-field approach that permits to visualize the exact solutions graphically as phase portraits in phase space.[7] Despite the subsequent loss of integrability, this formalism can be extended to higher numbers of order parameters and therefore provides an adequate framework to study the influence of the presence of solvent on the phase equilibria of thin films of polymer blend solutions. The advantage of this method is 2-fold: on one hand it will allow us to benefit from the technology of nonlinear dynamical systems and, on the other, it will render the comparison between the new solutions that we will find and their solvent-free counterparts−if any−more transparent, thus providing a direct insight on the influence of solvent.

Understanding the thermodynamical equilibrium of thin films of polymer blend solutions is of great practical importance as one of the most widely used methods of making very smooth, submicrometer thickness polymer films is solvent casting. When a polymer-blend solution is used, the two polymers will usually phase separate as solvent is removed, due to their low entropy of mixing. Many possible morphologies can result from the process, depending on the casting conditions. Usually, the phase-separated structure is found to be exclusively in the plane of the film, resulting in a laterally (or vertically) phase-separated film.[8] Of course, the formation of structures parallel to the surface of the film, with the formation of wettinglayers, is also observed.[9,10] This is known to occur in as-cast films of both PS/PMMA and PS/PB blends. Recently, the formation of a transient wetting layer has even been observed by *in situ* light scattering during the spin-coating process of PS/PMMA blends.[11] The bilayer subsequently breaks up through an interfacial instability with a wavelength selection mechanism,[12] leading to a final laterally phase separated morphology. From a technological point of view, the use of spin-coating to design polymer films for organic electronics is very attractive, as this technique combines simplicity, low cost, and versatility. Understanding the mechanisms of structure formation would allow one to gain some degree of control on the final polymer morphologies and, therefore, to design more complex and optimized nanostructures.

Of course the large variety of morphologies that can be reached during the spin-coating process is due to the fact that phase separation is controlled not only by the thermodynamics but also by the kinetics. Indeed, the fast removal of solvent can freeze out of equilibrium states and relaxation toward equilibrium may thus be hindered by kinetic barriers formed by the nonequilibrium phase morphology. In this paper, however, we will focus on the thermodynamics of thin films of polymer blend solutions, investigating in particular the influence of the film thickness and of the overall quantity of solvent on the actual equilibrium configuration of the system. This shall shed light on the different kinds of morphologies likely to appear during the spin-coating process itself and thus constitutes a first step toward a fully dynamical treatment of the problem.

The paper is organized as follows. In the second section, we define the Flory−Huggins−de Gennes free energy of a polymer-blend solution thin film, with additional interfacial terms. We then derive the corresponding Euler−Lagrange equations and the associated boundary conditions, which the equilibrium

*To whom correspondence should be addressed. E-mail: mireille.souche@durham.ac.uk.

Published on Web 05/25/2010

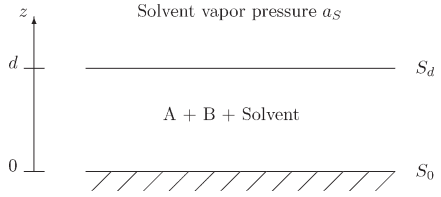

Figure 1. Physical setup.

concentration profiles are solutions of. We then turn to the Hamiltonian formulation of the problem in section 3, by deriving the expression of the Hamiltonian flow and of the boundary conditions in the phase space. We then present and discuss our numerical results in section 4, in the special case of walls that are antisymmetric for both polymers and symmetric for the solvent. We finally conclude in section 5.

2. Thermodynamics of Polymer Blend Solutions

2.1. Free Energy of the System. We consider a parallel-plate geometry of infinite area and width d, as depicted in Figure 1. A blend solution of polymers A and B in a common solvent S is at thermodynamical equilibrium with a vapor of solvent at activity $a_S = P_{vs}/P_0$. The activity a_S is the ratio of the saturated vapor pressure P_{vs} of the solvent at equilibrium with the solution to the saturated vapor pressure P_0 of the pure solvent. The chemical potential of the solvent vapor can be approximated to $\mu_{SV} \approx \mu^0_{SV} + k_B T \log[a_s] \equiv \mu_S k_B T$. It will be assumed that the solvent vapor consitutes a solvent reservoir, thus imposing its solvent chemical potential throughout the solution at thermodynamical equilibrium.

In this paper, z will denote the vertical coordinate and we shall denote by $\dot{g}$ the derivative wrt z of any function g of z. The film is bounded by two interfaces: one at $z = 0$, denoted S_0, and one at $z = d$, denoted S_d. Coordinates parallel to these interfaces are denoted by the two-dimensional vector $\mathbf{r}$.

The total free energy of the system is given by:

$$\mathscr{F} = \mathscr{F}_{bulk} + \mathscr{F}_{S_0} + \mathscr{F}_{S_d} \tag{1}$$

where $\mathscr{F}_{bulk}$ is the free energy associated with the bulk and $\mathscr{F}_{S_0}$ (respectively $\mathscr{F}_{S_d}$) that are associated with the interface S_0 (respectively S_d). Working in the grand-canonical ensemble, we write

$$\frac{\mathscr{F}_{bulk}}{k_B T} = a^{-3} \int \mathrm{d}^2 r \int_0^d \mathrm{d}z \left[-\mu_S \phi_s + f_{FH}(\phi_A, \phi_B, \phi_S) + \frac{a^2}{36}\left(\frac{1}{\phi_A}(\nabla\phi_A)^2 + \frac{1}{\phi_B}(\nabla\phi_B)^2 + \frac{1}{\phi_S}(\nabla\phi_S)^2\right)\right] \tag{2}$$

where the first term on the rhs accounts for the control of the solvent volume fraction by μ_{SV}. The second term, namely f_{FH}, represents the Flory−Huggins free energy, and is given by

$$f_{FH}(\phi_A, \phi_B, \phi_S) = \frac{\phi_A}{N_A}\ln(\phi_A) + \frac{\phi_B}{N_B}\ln(\phi_B) + \phi_S \ln(\phi_S) + \chi_{AB}\phi_A\phi_B + \chi_{AS}\phi_A\phi_S + \chi_{BS}\phi_B\phi_S \tag{3}$$

ϕ_A, ϕ_B, and ϕ_S being the volume fractions of the components A, B, and S, respectively. N_A is the degree of polymerization of polymer A and, likewise, N_B is that of polymer B. χ_{AB}, χ_{AS} and χ_{BS} are the interaction parameters between polymers A and B, polymer A and solvent, and polymer B and solvent, respectively. Finally, the last three terms are thus added to express the free-energy cost of having composition gradients. a denotes the spacing of the Flory−Huggins lattice. It is worth stressing that, as shown in recent works,[13−16] this mean-field theoretical description is no longer valid when the thickness of the film is much smaller than the gyration radius of the chains considered.

The incompressilibity of the solution is assumed, so that the variables (ϕ_A, ϕ_B, ϕ_S) are related by $\phi_A + \phi_B + \phi_S = 1$. Therefore, only two of the concentrations are independent variables. In what follows, we shall choose ϕ_A and ϕ_B and denote by $\mathscr{L}(\phi_A, \phi_B, \dot{\phi}_A, \dot{\phi}_B)$ the bulk free energy density.

The *bare* surface free energies $\mathscr{F}_{S_0}$ and $\mathscr{F}_{S_d}$ are added to $\mathscr{F}_{bulk}$ in order to account for the effect of the interfaces S_0 and S_d, respectively. We will assume that this effect is, at most, of order two in local compositions at the interfaces, so that, neglecting constant terms,

$$\frac{\mathscr{F}_{S_0}}{k_B T} = a^{-2}\int_{S_0} \mathrm{d}^2 r \left[-h^0_A \phi_{A0} - h^0_B \phi_{B0} - \frac{1}{2}\left(g^0_A \phi^2_{A0} + g^0_B \phi^2_{B0} + 2g^0_{AB}\phi_{A0}\phi_{B0}\right)\right] \tag{4}$$

$$\frac{\mathscr{F}_{S_d}}{k_B T} = a^{-2}\int_{S_d} \mathrm{d}^2 r \left[-h^d_A \phi_{Ad} - h^d_B \phi_{Bd} - \frac{1}{2}\left(g^d_A \phi^2_{Ad} + g^d_B \phi^2_{Bd} + 2g^d_{AB}\phi_{Ad}\phi_{Bd}\right)\right] \tag{5}$$

ϕ_{A0} (respectively ϕ_{B0}) and ϕ_{Ad} (respectively ϕ_{Bd}) represent the local volume fractions of polymer A (respectively B) at the interfaces S_0 and S_d, respectively. The coefficients h^0_i are phenomenological dimensionless parameters. Following reference 17, these coefficients can be related to observable quantities as follows

$$g_A = \frac{\zeta'}{\zeta}\chi_{AS}, \quad g_B = \frac{\zeta'}{\zeta}\chi_{BS}, \quad g_{AB} = \frac{\zeta'}{2\zeta}(\chi_{AS} + \chi_{BS} - \chi_{AB}) \tag{6}$$

$$h_A = -\frac{\zeta'}{2\zeta}\chi_{AS} + \frac{a^2}{k_B T}(\gamma_S - \gamma_A), \quad h_B = -\frac{\zeta'}{2\zeta}\chi_{BS} + \frac{a^2}{k_B T}(\gamma_S - \gamma_B) \tag{7}$$

where γ_A is the surface energy of component A (and likewise for B and S), ζ the coordination number of the lattice and ζ' the number of bonds that need to be cut to create an interface.

In the following, the energies will be normalized to $k_B T$ and the lengths to a.

2.2. Euler−Lagrange Equations and Boundary Conditions. The equilibrium volume−fraction profiles are those for which the free-energy of the system is minimized. For the sake of simplicity, we will neglect the inhomogenetities in the directions parallel to the interfaces and therefore assume that all functions only depend on z. The corresponding equilibrium

volume−fraction profiles are thus solutions of the following Euler−Lagrange equations:

$$\frac{\delta f}{\delta \phi_A} - \frac{\delta \kappa}{\delta \phi_A}(\phi_A)\,\dot{\phi_A}^2 - 2\kappa(\phi_A)\,\ddot{\phi}_A + \frac{\delta \kappa}{\delta \phi_S}(1-\phi_A-\phi_B)(\ddot{\phi}_A+\ddot{\phi}_B)^2 - 2\kappa(1-\phi_A-\phi_B)(\phi_A+\phi_B) = 0 \quad (8)$$

$$\frac{\delta f}{\delta \phi_B} - \frac{\delta \kappa}{\delta \phi_B}(\phi_B)\,\dot{\phi_B}^2 - 2\kappa(\phi_B)\,\ddot{\phi}_B + \frac{\delta \kappa}{\delta \phi_S}(1-\phi_A-\phi_B)(\dot{\phi_A}+\dot{\phi_B})^2 - 2\kappa(1-\phi_A-\phi_B)(\ddot{\phi}_A+\ddot{\phi}_B) = 0 \quad (9)$$

The function κ is defined by $\kappa(x) = 1/(36x^2)$, and the function f by $f = f_{FH} - \mu_S\phi_S$. This system of two order two ODEs is completed by four boundary conditions: two at $z = d$

$$2\kappa(\phi_A(d))\dot{\phi_A}(d) + 2\kappa(1-\phi_A(d)-\phi_B(d))(\dot{\phi_A}(d)+\dot{\phi_B}(d)) - h_A^d - g_A^d\phi_A(d) - g_{AB}^d\phi_B(d) = 0 \quad (10)$$

$$2\kappa(\phi_B(d))\dot{\phi_B}(d) + 2\kappa(1-\phi_A(d)-\phi_B(d))(\dot{\phi_A}(d)+\dot{\phi_B}(d)) - h_B^d - g_B^d\phi_B(d) - g_{AB}^d\phi_A(d) = 0 \quad (11)$$

and two at $z = 0$

$$2\kappa(\phi_A(0))\dot{\phi_A}(0) + 2\kappa(1-\phi_A(0)-\phi_B(0))(\dot{\phi_A}(0)+\dot{\phi_B}(0)) + h_A^0 + g_A^0\phi_A(0) + g_{AB}^0\phi_B(0) = 0 \quad (12)$$

$$2\kappa(\phi_B(0))\dot{\phi_B}(0) + 2\kappa(1-\phi_A(0)-\phi_B(0))(\dot{\phi_A}(0)+\dot{\phi_B}(0)) + h_B^0 + g_B^0\phi_B(0) + g_{AB}^0\phi_A(0) = 0 \quad (13)$$

Using the identity

$$\frac{d}{dz}[\kappa(\phi_i)\dot{\phi_i}^2] = \dot{\phi_i}(2\kappa(\phi_i)\ddot{\phi} + \frac{\delta\kappa}{\delta\phi_i}\dot{\phi_i}^2) \quad (14)$$

the (eq 8) $\dot{\phi}_A$ + (eq 9) $\dot{\phi}_B$ can be integrated to

$$\kappa(\phi_A)\dot{\phi_A}^2 + \kappa(\phi_B)\dot{\phi_B}^2 + \kappa(1-\phi_A-\phi_B)(\dot{\phi_A}+\dot{\phi_B})^2 - [f_{FH} - \mu_S(1-\phi_A-\phi_B)] = h \quad (15)$$

where h is an integration constant. The system of differential equations (eqs 8 and 9) thus admits a first integral of motion. It therefore constitutes a Hamiltonian dynamical system. In the next section, we switch from the present Lagrangian point of view, in which the system's Lagrangian is given by the bulk free energy (eq 2), to a Hamiltonian description of the system by means of a Legendre transformation.

3. Hamiltonian Formalism

3.1. Hamiltonian Flow and Boundary Conditions. *Hamiltonian Derivation.* While the Lagrangian description of the system is in terms of the generalized coordinates $q_1 = \phi_A$, $q_2 = \phi_B$ and of the generalized velocities $\dot{q}_1 = \dot{\phi}_A$, $\dot{q}_2 = \dot{\phi}_B$, in the Hamiltonian description the latter are replaced by the generalized momenta p_1 and p_2, defined by

$$p_i = \frac{\partial \mathscr{L}}{\partial \dot{q}_i}$$

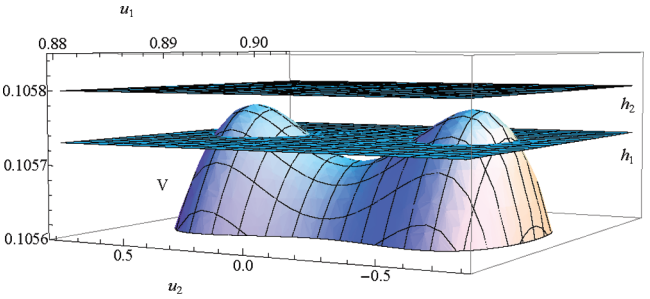

Figure 2. Decomposition of the Hamiltonian into potential and kinetic energy. The planes are H = constant, for two different values of constant (h_1 and $h_2 > h_1$) and the saddle-shape surface is $V(u_1,u_2)$. For all (u_1,u_2), the kinetic energy is given by $T(u_1,u_2) = H - V(u_1,u_2)$.

For the Lagrangian defined in (eq 2), we have

$$p_1 = 2\kappa(q_1)\dot{q}_1 + 2\kappa(1-q_1-q_2)(\dot{q}_1+\dot{q}_2),$$
$$p_2 = 2\kappa(q_2)\dot{q}_2 + 2\kappa(1-q_1-q_2)(\dot{q}_1+\dot{q}_2) \quad (16)$$

The Hamiltonian function, defined as a function of the $2n$ independent variables q_i and p_i, is given by

$$H(q_1,q_2,p_1,p_2) \equiv p_1\dot{q}_1 + p_2\dot{q}_2 - L(q_1,q_2,\dot{q}_1,\dot{q}_2) \quad (17)$$

$$= 9[q_1(1-q_1)p_1^2 - 2q_1q_2p_1p_2 + q_2(1-q_2)p_2^2] - [f_{FH}(q_1,q_2) - \mu_S(1-q_1-q_2)] \quad (18)$$

By construction, the latter is a first integral of motion, as derived in the previous section. By analogy with classical mechanics,[18] we write

$$H(q_1,q_2,p_1,p_2) = T(q_1,q_2,p_1,p_2) + V(q_1,q_2) \quad (19)$$

where the kinetic energy

$$T(q_1,q_2,p_1,p_2) = 9[q_1(1-q_1)p_1^2 - 2q_1q_2p_1p_2 + q_2(1-q_2)p_2^2] \quad (20)$$

is positive-definite and the potential energy is given by

$$V(q_1,q_2) = -[f_{FH}(q_1,q_2) - \mu_S(1-q_1-q_2)] \quad (21)$$

Figure 2 represents the typical shape of V as a function of ($u_1 = q_1 + q_2$, $u_2 = q_1 - q_2$). The kinetic energy can be obtained, at any value of (u_1,u_2), by subtracting V from the constant total energy. This implies, in particular, that, in Figure 2, the regions of the planes H = constant under V are forbidden.

Phase Portrait and Boundary Conditions. The phase portrait is then given by Hamilton's equations:

$$\dot{q}_1 = \frac{\partial H}{\partial p_1} = 18[q_1(1-q_1)p_1 - q_1q_2p_2] \quad (22)$$

$$\dot{q}_2 = \frac{\partial H}{\partial p_2} = 18[q_2(1-q_2)p_2 - q_1q_2p_1] \quad (23)$$

$$\dot{p}_1 = -\frac{\partial H}{\partial q_1}$$
$$= -9[(1-2q_1)p_1^2 - 2q_2p_1p_2] + \frac{\partial f}{\partial q_1}(q_1,q_2) \quad (24)$$

$$\dot{p}_2 = -\frac{\partial H}{\partial q_2}$$

$$= -9[(1-2q_2)p_2^2 - 2q_1p_1p_2] + \frac{\partial f}{\partial q_2}(q_1, q_2) \qquad (25)$$

Whereas Euler−Lagrange's equations are a set of n second-order differential equations, Hamilton's equations constitute a set of $2n$ first-order equations. These describe the possible evolutions of the system as trajectories, or phase portrait, in phase space. Among these, the appropriate solutions will be selected by the requirement that they meet the boundary conditions (eq 10−13). In the present formalism, the latter reduce to

$$p_{1,d} - h_A^d - g_A^d q_{1,d} - g_{AB}^d q_{2,d} = 0,$$
$$p_{2,d} - h_B^d - g_B^d q_{2,d} - g_{AB}^d q_{1,d} = 0 \qquad (26)$$

$$p_{1,0} + h_A^0 + g_A^0 q_{1,0} + g_{AB}^0 q_{2,0} = 0,$$
$$p_{2,0} + h_B^0 + g_B^0 q_{2,0} + g_{AB}^0 q_{1,0} = 0 \qquad (27)$$

where $q_{i,0}$ and $p_{i,0}$ (respectively $q_{i,d}$ and $p_{i,d}$) denote the values of the generalized coordinate and conjugate momentum $i = 1, 2$ at the boundary $z = 0$ (respectively $z = d$). From the point of view of the four dimensional phase space, these boundary conditions are located on 2-planes.

Change of Coordinates. We now introduce a new coordinatisation of phase space that will be particularly convenient in the forthcoming sections, as it is more adapted to the symmetries of the potential. We let $u_1 = q_1 + q_2$, $u_2 = q_1 - q_2$, $v_1 = p_1 + p_2$ and $v_2 = p_1 - p_2$. In terms of these, the Hamiltonian becomes

$$H(u_1, u_2, v_1, v_2) = \frac{9}{4}u_1(1-u_1){v_1}^2 + \frac{9}{2}u_2(1-u_1)v_1v_2$$
$$+\frac{9}{4}(u_1 - {u_2}^2){v_2}^2 - f(u_1, u_2) \qquad (28)$$

$$\equiv T(u_1, u_2, v_1, v_2) + V(u_1, u_2) \qquad (29)$$

The case without solvent, $u_1 = 1$, reproduce the equation of the phase portrait in two polymer mixtures.[7] The derivation of the flow equations and boundary conditions in this new set of coordinates is straightforward and will not be reproduced here.

3.2. Equations in the H = Constant Space. The phase space introduced in the previous section is four-dimensional and it will be convenient, for graphical purposes, to restrict the flow and the boundary conditions to some three-dimensional subspace. Since H is a conserved quantity along the flow, a natural way to do so consists in restricting to the three-dimensional spaces of constant H.

Equations for the Flow. It follows from the expression of the Hamiltonian, (eq 28), that, at any fixed value of (u_1,u_2), $H_{u_1,u_2}(v_1,v_2)$ = constant describes an ellipse in the plane spanned by the coordinates v_1 and v_2. For every value of (u_1,u_2), this ellipse can be parametrized piecewise by v_2, with

$$v_1 = -\frac{u_2}{u_1}v_2 + \frac{2\sqrt{\Delta(u_1, u_2, v_2)}}{9u_1(1-u_1)}$$

in the upper branch of the ellipse and

$$v_1 = -\frac{u_2}{u_1}v_2 - \frac{2\sqrt{\Delta(u_1, u_2, v_2)}}{9u_1(1-u_1)}$$

in the lower one, where

$$\Delta(u_1, u_2, v_2) = \frac{9}{4}(1-u_1)[4u_1(f(u_1, u_2) + h) - 9{v_2}^2({u_1}^2 - {u_2}^2)]$$
$$\equiv \frac{9}{4}(1-u_1)\delta(u_1, u_2, v_2) \qquad (30)$$

For all (u_1,u_2), the two branches of the ellipse overlap at $v_2 = v_2^{\pm}$ such that $\Delta(u_1,u_2,v_2^{\pm}) = 0$, i.e.

$$v_2^{\pm}(u_1, u_2) = \pm\sqrt{\frac{4}{9}\frac{u_1}{{u_1}^2 - {u_2}^2}(f(u_1, u_2) + h)} \qquad (31)$$

The space $H(u_1,u_2,v_1,v_2)$ = constant can thus be thought of as a couple of overlapping three-dimensional compact spaces of coordinates (u_1,u_2,v_2), one for each branch of the ellipse in the plane (v_1,v_2), which we shall, by extension, refer to as branches. The three-dimensional branch corresponding to the upper (respectively lower) branch of the ellipse will be referred to as the + (respectively −) branch. These are identified at their boundaries $(u_1,u_2,v_2^{\pm}(u_1,u_2))$, i.e. across the surface $\Delta = 0$. Note that, although a polar parametrization of the ellipse would have provided a single-chart description, it is highly inconvenient as it makes the dynamics much more complicated. For this reason it has not been used here.

In terms of (u_1,u_2,v_2), the flow is reduced, in each branch, to

$$\dot{u}_1 = \pm 3\sqrt{(1-u_1)\delta(u_1, u_2, v_2)} \qquad (32)$$

$$\dot{u}_2 = 9\left[\left(u_1 - \frac{{u_2}^2}{u_1}\right)v_2 \pm \frac{u_2}{3u_1}\sqrt{(1-u_1)\delta(u_1, u_2, v_2)}\right] \qquad (33)$$

$$\dot{v}_2 = 2\partial_{u_2}f - 9\left[-\frac{u_2}{u_1}v_2^2 \pm \frac{v_2}{3u_1}\sqrt{(1-u_1)\delta(u_1, u_2, v_2)}\right] \qquad (34)$$

For $u_1 = 1$, the last two equations above reproduce the phase portrait for polymer blends without solvent,[7] This case will be discussed in more detail in the next section, where we describe the general features of the flow.

General Shape of the Flow. Let us first specify the accessible domain of (u_1,u_2,v_2) in the space $H(u_1,u_2,v_1,v_2)$ = constant. On one hand, the positivity of T in eq 28 allows to determine the accessible values of (u_1,u_2) for all H. On the other, the positivity of Δ (eq 30), required to obtain real roots when solving for v_1 in terms of v_2, implies that

$$v_2^-(u_1, u_2) \le v_2 \le v_2^+(u_1, u_2) \qquad (35)$$

Note that if $T > 0$ for all points in $H(u_1,u_2,v_1,v_2)$ = constant, the surfaces described by $v_2 = v_2^{\pm}(u_1, u_2)$ are disconnected. They can thus only intersect at points where $T = 0$, see Figure 3.

To obtain a better understanding of the structure of the flow, we shall discuss separately its longitudinal component along u_1, described by eq 32, and its transverse component in the plane (u_2,v_2), described by eqs 33 and 34.

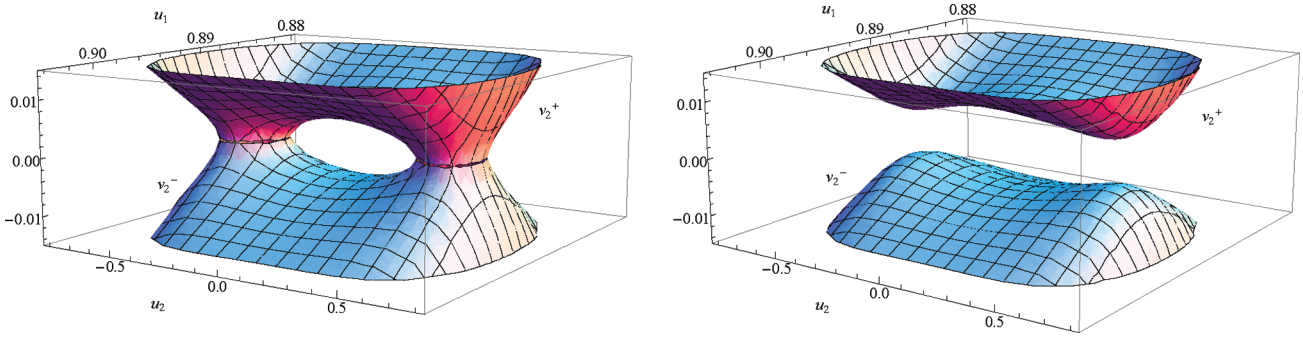

Figure 3. Surface $\Delta(u_1,u_2) = 0$ for $H = h_1$ on the left and $H = h_2$ on the right, with h_1 and h_2 defined in Figure 2.

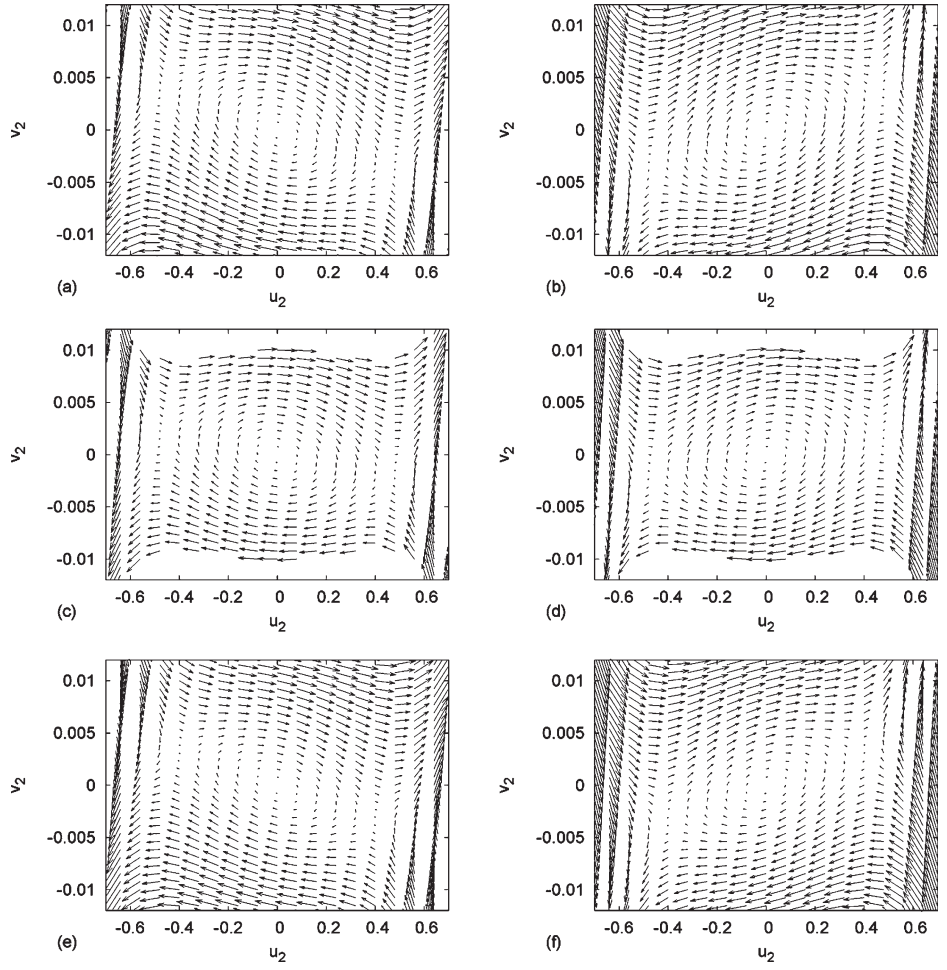

Figure 4. Projection of the Hamiltonian flow in the (u_2,v_2) planes in the case $H > V_{\max}$, for different values of u_1: (a, b) $u_1 \simeq u_{1,max} + 0.01$, (c, d) $u_1 \simeq u_{1,max}$, (e, f) $u_1 \simeq u_{1,max} - 0.01$, where $u_{1,min}$ maximizes V. The left column corresponds to the + branch, the right one to the − branch.

First, the longitudinal component has definite sign in each branch and changes sign from one branch to the other. It vanishes precisely at $\Delta = 0$, which is on the union of the surfaces respectively defined by $u_1 = 1$ and $\Delta = 0$. The picture is therefore that of a trajectory evolving toward $\Delta = 0$ in one branch and then bouncing back from it in the other branch; except at the intersection of $u_1 = 1$ and $\Delta = 0$, which actually reproduces the solution without solvent. In the latter case, u_1 actually remains constant equal to 1.

In addition to this longitudinal component, the transverse component consists of an integrated motion through the layers u_1 = contant for a range of values of the constant. Figure 4 and Figure 5 depict the projections of the Hamiltonian flow at different values of u_1. In Figure 4, $H > V_{\max}$ is assumed, whereas in Figure 5, $V_0 < H \leq V_{\max}$ resulting in the existence of a forbidden region which corresponds to the empty stripes on the graphs of the second line. It is worth noting that the shape of the projected flow constitutes a deformation of the integrable two-dimensional flow familiar from the solvent-free case, $u_1 = 1$. In particular, although the outermost envelope of each graph remains undeformed, the flow inside this envelope gets tilted, clockwise in the + branch, counterclockwise in the − branch. Furthermore, as u_1 departs from its most favored value, the concentric ellipses get contracted toward the center of the graph, until they eventually disappear.

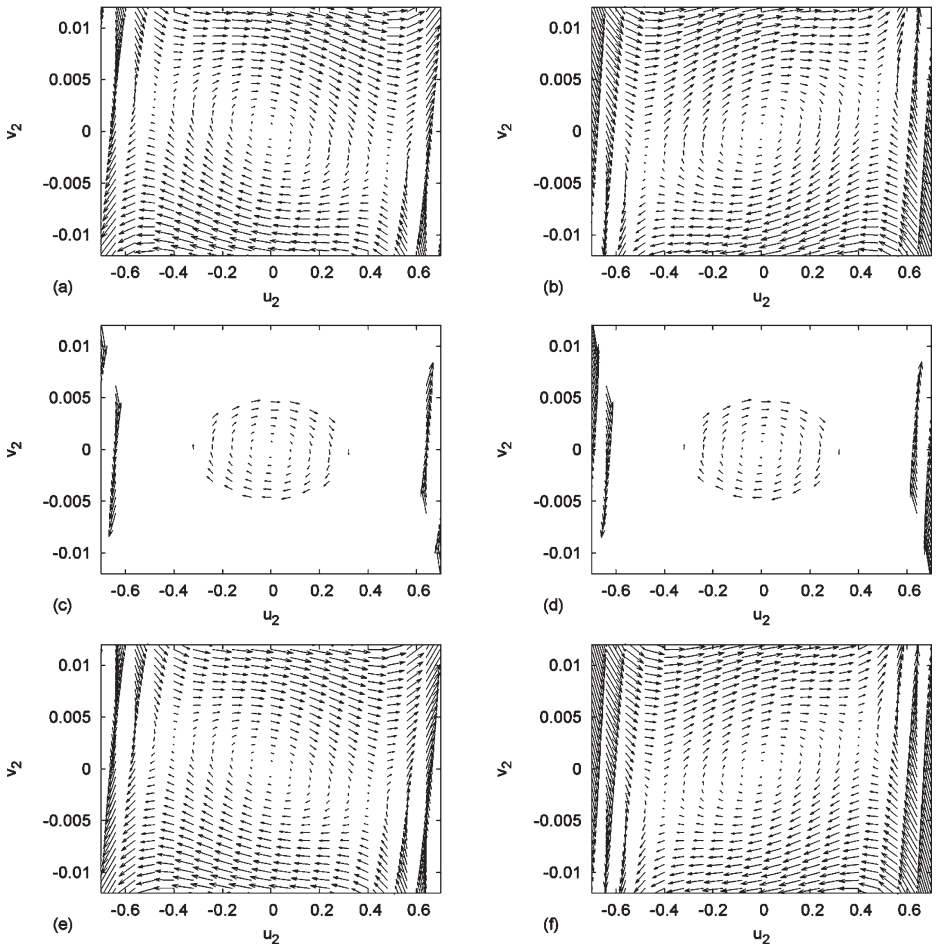

Figure 5. Projection of the Hamiltonian flow in the (u_2,v_2) planes in the case $V_0 < H \leq V_{\max}$, for different values of u_1: (a, b) $u_1 \simeq u_{1,max} + 0.01$, (c, d) $u_1 \simeq u_{1,max}$, (e, f) $u_1 \simeq u_{1,max} - 0.01$. The left column corresponds to the + branch, the right one to the − branch.

Boundary Conditions. In phase space, the boundary conditions at $z = 0$ or d are the intersections of the two three-dimensional hyperplanes respectively defined by

$$\begin{aligned} v_1^0 + h_1^0 + g_1^0 u_1^0 + g_{12}^0 u_2^0 &= 0, \\ v_2^0 + h_2^0 + g_2^0 u_2^0 + g_{12}^0 u_1^0 &= 0 \end{aligned} \tag{36}$$

$$\begin{aligned} v_1^d - h_1^d - g_1^d u_1^d - g_{12}^d u_2^d &= 0, \\ v_2^d - h_2^d - g_2^d u_2^d - g_{12}^d u_1^d &= 0 \end{aligned} \tag{37}$$

It follows that these intersections can be parametrized by the coordinates (u_1,u_2). Restricted to the space $H(u_1,u_2,v_1, v_2) =$ constant, they become one-dimensional curves whose projections in the (u_1,u_2)-plane are implicitly given by $H(u_1, u_2,v_1^i,v_2^i) =$ constant, for $i = 0$ or d. The corresponding values of v_1 and v_2 being determined by eqs 36 and 37, each of the boundary conditions lies in a definite branch. Let us note that, if we assume that $g_A^i = g_B^i$, which is reasonable in a symmetric solution (see eq 6), the coefficients g_{12}^i are equal to zero. This means that the projection of the one-dimensional boundary curve in (u_2,v_2)-plane is along a line; see Figure 9.

4. Numerical Results and Discussion

4.1. Introduction. In this section, we focus on the special case of walls that are antisymmetric for both polymers and symmetric for the solvent. Technically, this implies that $h_1^0 = h_1^d$ and $h_2^0 = -h_2^d$. Furthermore, the polymer−polymer-solvent mixture is assumed to be symmetric, *i.e.*, $N_A = N_B = N$ and $\chi_{AS} = \chi_{BS} = \chi$. The critical solvent concentration is thus equal to $\phi_{Sc} = 1-2/(N\chi)$.

Before presenting our results, let us first discuss the numerical method we used. Solutions are found by shooting: each point of the $z = 0$ boundary curve is numerically evolved following the Hamiltonian flow and the resulting trajectory is considered a solution if and only if it intersects the boundary curve at $z = d$ in the $H = constant$ space to the desired accuracy. Numerical integration of the Hamilton equations is performed by adaptative stepsize fourth order Runge−Kutta method. A typical solution is depicted in Figure 6. The length of each solution is then obtained by numerical integration of the curvilinear coordinate z along the trajectory. As in reference 7, different values of the Hamiltonian H will usually yield solutions of different lengths.

Note finally that the system has only one conserved charge−the Hamiltonian−for 2 degrees of freedom−u_1 and u_2−allowing sensitivity of the Hamiltonian flow to the initial conditions. Technically, the appearance of such a behavior requires the use of high precision numbers in order to actually reach solutions to within a given precision bound.

Following the treatment of polymer blend thin films, the excess surface free-energy is defined by

$$\sigma(d) = F(d) - d \times f(\phi_A^{bulk}, \phi_B^{bulk}) \tag{38}$$

which, using the constant of H, can be written as follows:

$$\begin{aligned} \sigma(d) = F_{S_0}(\phi_A^0, \phi_B^0) + F_{S_d}(\phi_A^d, \phi_B^d) - d[f(\phi_A^{bulk}, \phi_B^{bulk}) - H] \\ + 2\int_0^d \mathrm{d}z\, f(\phi_A(z), \phi_B(z)) \end{aligned} \tag{39}$$

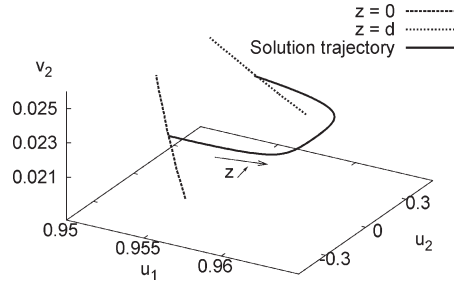

Figure 6. Determination of a solution trajectory (bold line) in the (u_1,u_2,v_2) space, where boundary conditions are represented by curves (dashed lines).

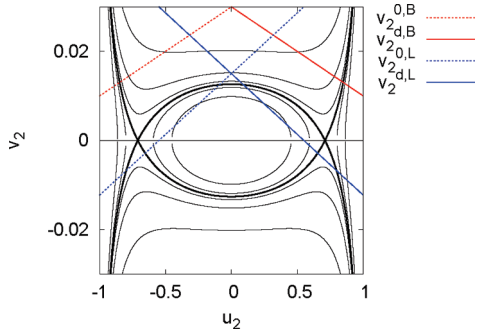

Figure 7. Visualization of equilibrium concentration profiles of polymer blend thin film in terms of trajectory in the phase space: for $T > T_w$, bilayer structure (boundary conditions $v_2^{0,B}$ and $v_2^{d,B}$, in red); for $T < T_w$, lateral phase separated structure (boundary conditions $v_2^{0,L}$ and $v_2^{d,L}$, in blue).

In particular, in the case of many solutions for a given thickness, the stable one will be the one with the lowest σ.

We now discuss two cases: $T > T_w$, in section 4.2, and $T < T_w$, in section 4.3, where T_w denotes the wetting temperature for polymers. We shall pay particular attention to the role of μ_S, i.e. to the quantity of solvent in the film. For binary polymer blends, the corresponding solutions are well-known[19,20] and their description in phase space was given by the present authors in reference 7.

4.2. $T > T_w$: The Monolayer/Bilayer Transition. To begin with, we consider the case $T > T_w$. More precisely, we use the following numerical values: $N = 100$, $\chi = 0.3$, $\chi_{AB} = 0.025$, $h_1^0 = h_1^d = 0.09$ and $h_2^0 = -h_2^d = -0.03$, $g_1^0 = g_1^d = -0.18$, $g_2^0 = g_2^d = -0.02$ and $g_{12}^0 = g_{12}^d = 0$. In this case, whatever the thickness of the film, the equilibrium configuration of a solvent-free polymer blend thin film is a bilayer, characterized by the existence of a local maximum of the function $\dot{u}_2(u_2)$, reached when $u_2 = 0$ for symmetric films. Note that, although there can be a discrepancy between the numbers of minima and maxima of $v_2(u_2)$ and $\dot{u}_2(u_2)$, we shall only consider situations in which they agree, making it easier to identify the nature of the solutions directly from the shape of the phase portraits. Typical phase portraits are depicted in Figure 7 for such situations. They agree with the results obtained for polymer blend solutions in the limit $\mu_S \to -\infty$.

Figure 8 represents the deformation of the phase portraits as μ_S is increased. For each value of μ_S, four solutions are depicted, corresponding to various thicknesses of the film. It is obvious from this figure that, as the amount of solvent increases, the phase portraits undergo a transition from two minima and a maximum to a single minimum in v_2. As a consequence, the systems evolves from a bilayer, in the absence of solvent and at low μ_S, to a monolayer as the amount of solvent increases. It is worth representing the above solutions as concentration profiles. An example is

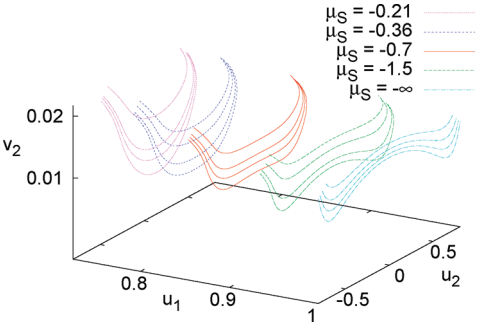

Figure 8. Deformation of the phase portrait with the chemical potential of solvent μ_S, for $T > T_w$.

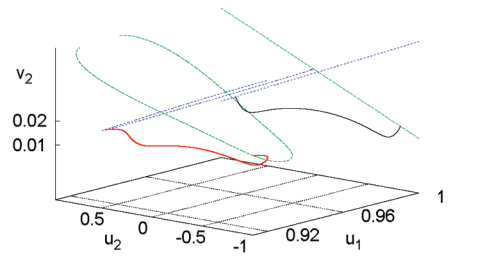

(a) In the (u_1,u_2,v_2)-space.

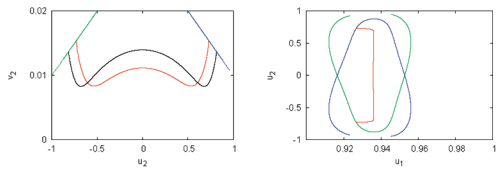

(b) Projection in the (u_2,v_2)-plane. (c) Projection in the (u_1,u_2)-plane.

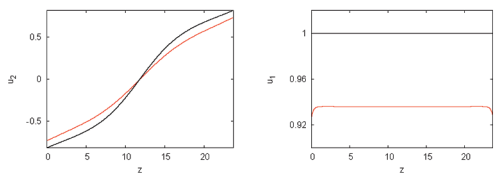

(d) Profiles in u_2 (e) Profiles in u_1

Figure 9. Representations of solutions of same length for two values of μ_S: $\mu_s = -1.5$ in red and $\mu_s = -\infty$ in black. Associated boundary conditions in $z = 0$ and $z = d$ are in green and blue, respectively.

shown in Figure 9. In particular, the solvent concentration as a function of z is better visualized in this way and it turns out to be almost constant throughout the film with excesses near the boundaries as shown in Figure 9e.

Figure 10 represents, for each of the solutions of Figure 8, the excess surface free energy σ as a function of the film thichness d. As in the case of polymer blends, for a given μ_S, σ is a decreasing function of d. Moreover, at a given thickness, the addition of solvent diminishes the excess surface free energy, resulting in a stabilization of the corresponding solutions. Note finally that the solutions on the $u_1 = 1$ plane always exist, even for finite values of μ_S (see eqs 32−34), but are energetically disfavored unless $\mu_S \to -\infty$, given that they have higher excess surface free energy.

4.3. $T < T_w$: the monolayer/bilayer/lateral phase separated film transition. We now turn to the case $T < T_w$. To be more precise, we use the following numerical values: $N = 100$, $\chi = 0.3$, $\chi_{AB} = 0.025$, $h_1^0 = h_1^d = 0.09$ and $h_2^0 = -h_2^d = -0.015$,

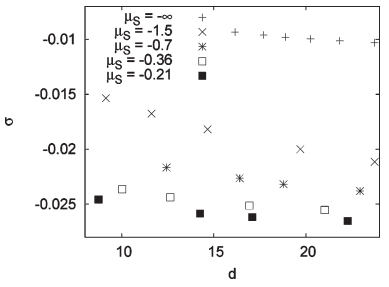

Figure 10. Dependance of the excess surface free energy σ of the solutions depicted in Figure 8 with the thickness of the film.

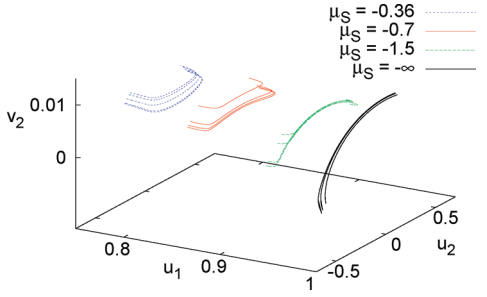

Figure 11. Deformation of the phase portrait with the chemical potential of solvent μ_S, for $T < T_w$. For clarity, in the cases $\mu_S = -\infty$ and $\mu_S = -1.5$, only one asymmetric solution has been depicted and the long symmetric solution has been omitted.[7].

$g_1^0 = g_1^d = -0.18$, $g_2^0 = g_2^d = -0.015/0.55$ and $g_{12}^0 = g_{12}^d = 0$. Thus, the values of the solvent interaction parameteres are kept unchanged as compared to the previous section.

The corresponding numerical solutions are presented as trajectories in phase space in Figure 11, for different values of the chemical potential of the solvent μ_S. In the limit $\mu_S \to -\infty$, we recover the solutions for polymer blend thin films with antisymmetric walls: for sufficiently thick films, two solutions coexist, resulting in a lateral phase separation (see Figure 7).

As μ_S increases, so does the total amount of solvent in the film and the phase portrait undergoes two transitions, in turn. First, the two coexisting solutions, corresponding to a lateral phase separation of the film, merge into a single solution characterized by the existence of two minima and a maximum and describing a bilayer structure in the film. The equilibrium structure of the film therefore evolves from lateral phase separation to a bilayer. This transition occurs at values of the solvent chemical potential that depend on the thickness of the film. Indeed, in the case of $\mu_s = -1.5$, we see that, for sufficiently thick films, two solutions coexist, while for thinner films, the structure is that of a bilayer Figure 12. Second, as the amount of solvent further increases, the equilibrium structures of the system become analogous to those observed for $T > T_w$: the bilayer, observed for $\mu_S = -0.7$, is replaced by a monolayer characterized by a single minimum in v_2 ($\mu_S = -0.36$). The distribution of the solvent throughout the film is similar to that described in the previous sections.

4.4. Unstable Solutions and Chaos. The solutions we have discussed so far are essentially "deformations" of known solutions for polymer blends without solvent in the sense that, despite exhibiting the nontrivial dynamics of the solvent concentration, they are in one-to-one correspondence with the latter. They are also energetically favored as they always remain near the minimum of the Flory−Huggins−de Gennes free energy. Now, it is worth commenting on the fact

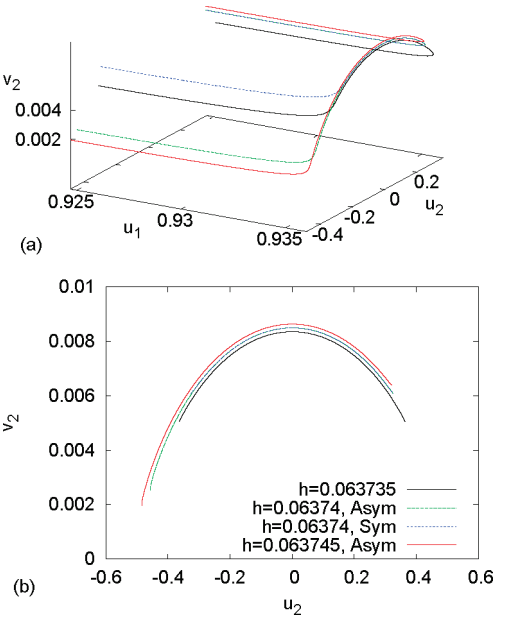

Figure 12. Deformation of the phase portrait for $\mu_S = -1.5$: (a) in the (u_1,u_2,v_2) space; (b) in the (u_2,v_2) plane.

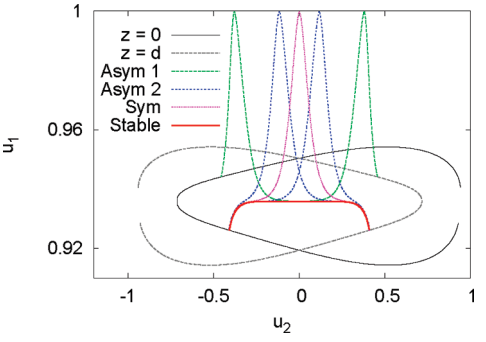

Figure 13. Representation of solutions in the (u_1,u_2)-plane in the case of $\mu_S = -1.5$, with parameter of section 4.2, at a given value of the Hamiltonian: as well as the stable solution (red) described in section 4.2, both symmetric (purple) and asymmetric solutions (green and blue) appear.

that the addition of an independent order parameter results in the appearance of genuinely new solutions with no analogues in the solvent free situation. In general, these are energetically disfavored as compared to the previously discussed solutions. Seen as an evolution problem, the system exhibits, in the vicinity of these solutions, a high sensitivity to initial conditions which might be the consequence of a chaotic behavior of the Hamiltonian flow in the concerned regions of phase space.

As an example, we now briefly discuss those solutions, which bounce on the plane $u_1 = 1$. Typical such solutions are depicted in Figure 13. The parameters used there are the same as those used for Figure 8, with $\mu_S = -1.5$ and the value of the Hamiltonian is kept constant. We see that both symmetric and asymmetric solutions, characteristic of lateral phase separation, appear. Their excess surface free energies are even higher than the ones of the solutions at $\mu_S \to -\infty$. It is also possible to consider solutions which bounce more than once between $u_1 = 1$ and $\Delta = 0$ (not represented in Figure 13) and which have higher excess free energies as they evolve even further from the minimum of the Flory−Huggins−de Gennes free energy. Although unstable, these solutions surely contribute to the out-of-equilibrium dynamics of the

system and therefore deserve further attention. Figure 13 also illustrates the sensitivity of the system to initial conditions near the boundary conditions of these solutions. Note in particular, that the solutions which bounce on the $u_1 = 1$ plane typically admit diverging values of v_1 near $u_1 = 1$, while the stable solutions remain strictly confined within a finite neighborhood. We postpone the study of these aspects and of a possible role of chaos therein to future publications.

5. Conclusion

In this article, we have studied the equilibrium concentration profiles in thin films of polymer blend solutions, as described by the Flory−Huggins free energy with quadratic boundary terms. We have first generalized the Hamiltonian description of polymer blend thin films from ref 7 to the case of polymer blend solutions. The addition of an independent order parameter, corresponding to an extra degree of freedom at the level of the Hamiltonian formulation of the theory as compared to the solvent free case, results in the loss of integrability of the system and, consequently, in the necessity of a numerical resolution.

The numerical solutions displayed were then derived by means of a shooting technique adapted to the phase space description. Particular attention has been paid to the role of the solvent in the special case of a polymer blend solution confined between two walls that are antisymmetric with respect to both polymers and symmetric with respect to the solvent. We have shown in particular that, whatever $T < T_c$, the system generically undergoes a transition from a roughly homogeneous monolayer structure with excess of solvent and of the favored polymer near each interface to a bilayer structure as solvent is removed from the solution. Furthermore, depending respectively on whether $T > T_w$ or $T < T_w$, the film either remains a bilayer or phase separates, thus acquiring a lateral structure orthogonal to the interfaces. It is worth mentioning that, for the values of the parameters chosen in this paper and, arguably, for all other physically relevant choices of these, new unstable solutions usually appear which may play some role in a dynamical description of the out-of-equilibrium behavior of the system.

References and Notes

(1) Müller, M.; Albano, E. V.; Binder, K. *Phys. Rev. E* **2000**, *62*, 5281–5295.
(2) Binder, K.; Müller, M.; Albano, E. V. *Phys. Chem. Chem. Phys.* **2001**, *3*, 1160–1168.
(3) Nakanishi, H.; Pincus, P. *J. Chem. Phys.* **1983**, *79*, 997–1003.
(4) Schmidt, I.; Binder, K. *J. Phys.* (*Paris*) **1985**, *46*, 1631–1644.
(5) Flebbe, T.; Dünweg, B.; Binder, K. *J. Phys. II* **1996**, *6*, 667–695.
(6) Eggleton, C. D. *Phys. Lett. A* **1996**, *223*, 394–399.
(7) Souche, M.; Clarke, N. *J. Chem. Phys.* **2009**, *131*, 244903.
(8) Krausch, G.; Kramer, E. J.; Rafailovich, M. H.; Sokolov, J. *Appl. Phys. Lett.* **1994**, *64*, 2655–2657.
(9) Geoghegan, M.; Jones, R. A. L.; Payne, R. S.; Sakellariou, P.; Clough, A. S.; Penfold, J. *Polymer* **1994**, *35*, 2019–2027.
(10) Walheim, S.; Böltau, M.; Steiner, U.; Krausch, G. *Macromolecules* **1997**, *30*, 4995–5003.
(11) Heriot, S. Y.; Jones, R. A. L. *Nat. Mater.* **2005**, *4*, 782–786.
(12) Souche, M.; Clarke, N. *Eur. Phys. J. E* **2009**, *28*, 47–55.
(13) Semenov, A. N.; Johner, A. *Eur. Phys. J. E* **2003**, *12*, 469–480.
(14) Cavallo, A.; Müller, M.; Binder, K. *Europhys. Lett.* **2003**, *61*, 214–220.
(15) Cavallo, A.; Müller, M.; Binder, K. *J. Chem. Phys. B* **2005**, *109*, 6544–6552.
(16) Meyer, H.; Kreer, T.; Aichele, M.; Cavallo, A.; Johner, A.; Baschnagel, J.; Wittmer, J. P. *Phys. Rev. E* **2009**, *79*, 050802.
(17) Jones, R. A. L.; Richards, R. W. *Polymers at Surfaces and Interfaces*; Cambridge University Press: Cambridge, U.K., 1999.
(18) Kibble, T. W. B. *Classical mechanics*; Wiley: New York, 1985.
(19) Parry, A. O.; Evans, R. *Phys. Rev. Lett.* **1990**, *64*, 439–442.
(20) Parry, A. O.; Evans, R. *Physica A* **1992**, *181*, 250–296.